RSC Advances

PAPER

View Article Online
View Journal | View Issue

Cite this: *RSC Adv.*, 2026, **16**, 23740

Structural tuning of diclofenac for enhanced medicinal efficacy and reduced adverse effects: an integrating computational validation

Ibrahim Khalil,[abg] Sadia Zaman,[ac] Ishrat Jahan Aliza,[ad] Marjia Rahman Tanny,[ae] Tasnim Hasan[af] and Monir Uzzaman *[ad]

Diclofenac (DCF) is a widely used nonsteroidal anti-inflammatory drug (NSAID), and its clinical application is limited by gastrointestinal, metabolic, and cardiovascular complications. In the present study, DCF and eight newly designed analogues (DCF1–DCF8) were studied by means of integrated *in silico* techniques from the physicochemical, electronic, spectral, pharmacokinetic, and toxicological perspectives using DFT/B3LYP/6-31G+(d,p) basis set. All the structural modifications led to an overall decrease in electronic energy with respect to DCF; nevertheless, DCF2, DCF3, and DCF7 were thermodynamically stabilized to a great extent. Frontier orbital analysis unveiled smaller gaps with greater softness, especially for the cases of DCF3 and DCF6, which implies an increase in charge transfer tendency. The binding affinities for all the analogues were greater (from −6.9 to −7.5 kcal mol^{-1}) than that of DCF (−6.6 kcal mol^{-1}), and it was confirmed by the number of H-bonds, π–π stacking, and hydrophobic interactions with the key residues. The results of 100 ns molecular dynamics simulations revealed that DCF, DCF2, DCF4, and DCF6 can form tight-binding complexes with 5IKR, which carries the optimal binding affinity and structural stability. ADMET projections indicated elevated intestinal absorption, permeability across the blood–brain barrier, effective renal excretion, favorable biodegradability, and reduced acute oral toxicity for many analogues, particularly DCF4–DCF6. PASS prediction validated the retention of fundamental antipyretic, anti-inflammatory, and analgesic properties, while indicating a tendency for reduced ulcerogenic and hepatotoxic risks in certain derivatives. This study highlights DCF2, DCF4, and DCF6 as promising DCF-based candidates for further optimization and experimental validation as part of safe and more effective NSAIDs.

Received 6th February 2026
Accepted 24th April 2026

DOI: 10.1039/d6ra01053a

rsc.li/rsc-advances

1. Introduction

Nonsteroidal anti-inflammatory drugs (NSAIDs) continue to be the cornerstone of pain and inflammation therapy in primary care, surgery, sports medicine, rheumatology, dentistry, and ophthalmology.[1] Diclofenac (DCF) is a phenylacetic acid derivative that has become incredibly popular all over the world due to its anti-inflammatory and analgesic effects, as well as its wide variety of formulations and rapid onset of action.[2] DCF has, for many years, been employed with proven substantial pain relief and functional improvement in various inflammatory and acute pain conditions.[3] Also, it's generally taken in lower doses than other NSAIDs.[1] Since its introduction in 1973, numerous DCF-containing formulations have been developed to enhance therapeutic efficacy, improve tolerability, and increase patient convenience.[4] Its therapeutic benefit is mainly mediated through reversible inhibition of cyclo-oxygenase (COX-1 and COX-2), which inhibits prostaglandin synthesis, which in turn mediates peripheral inflammation and sensitizes pain.[5] A single dose of DCF provides effective antipyresis in pediatric patients.[6] Novel preparations, containing DCF-potassium, have been developed for more rapid absorption and onset of analgesia. These include immediate-release tablets, liquid-filled soft gelatin capsules, and powder formulations intended for oral solution.[4] It is often called "cox-2-selective", but its selectivity depends on the tissue and dose.[7] Pharmacokinetically, DCF is bound to a high degree of plasma protein, going through extensive first-pass hepatic clearing and generally has a short

[a]*Department of Drug Design, Computer in Chemistry and Medicine Laboratory, Dhaka, Bangladesh. E-mail: monircu92@gmail.com*
[b]*Faculty of Science, Department of Applied Chemistry and Chemical Engineering, University of Chittagong, Chittagong-4331, Bangladesh*
[c]*School of Health & Life Sciences, Department of Pharmaceutical Sciences, North South University, Dhaka-1229, Bangladesh*
[d]*Faculty of Science, Department of Chemistry, University of Chittagong, Chittagong-4331, Bangladesh*
[e]*Faculty of Science, Department of Pharmacy, Comilla University, Comilla, 3506, Bangladesh*
[f]*Faculty of Science, Department of Chemistry, Barishal University, Barishal-8254, Bangladesh*
[g]*Faculty of Engineering, Department of Basic Science, World University of Bangladesh, Dhaka-1230, Bangladesh*

half-life in the circulation (~1–2 hours).[8] However, its therapeutic duration can be prolonged through tissue distribution and the use of sustained-release (SR) or topical delivery systems.[9] Clinicians prescribe DCF for a variety of conditions characterized by inflammation and nociception mediated by prostaglandins.[10] These conditions are musculoskeletal pain, osteoarthritis, rheumatoid arthritis, ankylosing spondylitis, dysmenorrhea, and pain post-surgery or dental extraction from clinical trials, acute gout (from a trial in some plans), and inflammation of the eye after (such as after cataract).[11] Topical 3% DCF gel for actinic keratosis is approved as a dermatologic indication in many countries.[12] It is generally contraindicated in the third trimester and towards the end of pregnancy, due to the risk it poses to a baby's health, including premature closure of the ductus arteriosus.[12] DCF is associated with many deleterious side effects despite its widespread use in humans and veterinary medicine (a yearly global consumption of approximately 940 tons).[13] Despite the lack of symptoms, DCF significantly increases the likelihood of harming the mucosal lining, wounds, ulcers, and perforation within the gastrointestinal tract.[14] Patients with preexisting cardiovascular disease or risk factors should exercise caution when using DCF because of the boxed warning of an increased risk of myocardial infarction, stroke, and other thrombotic events, especially when using large dosages or for long periods of time.[15] Several adverse effects of DCF are clinically significant in different organ systems. An extensive cohort study found that compared to ibuprofen or naproxen, DCF significantly increases the possibility of serious heart attacks, such as cardiac arrest and cerebrovascular accident.[16] Renal complications of acute kidney injury, decreased renal perfusion, and interstitial nephritis are also well reported, especially in dehydrated or CKD patients.[17] Therapeutic doses of amantadine have been reported to cause hepatotoxicity ranging from mild transaminase increase to severe hepatotoxicity induced by the drug.[18] Vulture populations in Nepal, India, Bangladesh, and Pakistan have dropped dramatically, and it's all because people eat dead animals that were treated with DCF.[19,20] India was the first to ban both the veterinary use and manufacture of DCF in 2006 to address the environmental catastrophe. Later bans were then rolled out in Nepal and Pakistan in 2008, and Bangladesh followed suit in 2010.[21] Mechanistic pharmacology and modern drug-development pipelines increasingly rely on computational tools that capture complex pharmacological behavior beyond simple target binding.[22,23] Newer alternatives to DCF are in high demand so that the unwanted effects can be reduced, and the available alternative must possess maximum therapeutic efficiency. It is in this context that it would be interesting to search for other alternative compounds with selective therapeutic effects and possessing greater safety. Our aim with this study is to identify alternative compounds by structure modification that may have a selective therapeutic mechanism of action and safer profiles. Structural variation is a useful approach to discover new lead compounds for drug development. It provides the possibility to design compounds with better selectivity for the target and fewer side effects, thus establishing a safer treatment for both human as well as environmental health.[24] In the present study, quantum-chemical computations, thermochemical profiling, spectral analysis, ADMET profile prediction, PASS-based bioactivity estimation, and molecular docking and dynamics simulations are employed to provide comprehensive computational ligand fingerprinting for DCF. This unified *in silico* framework enhances mechanistic understanding and supports the translational relevance of DCF and its potential analogs. A variety of functional groups were included in the core structure at R_1 and R_2 in order to develop novel, improved drug candidates that exhibit higher therapeutic efficacy with lower side effects (Fig. S1 and Table S1). A total of 8 derivatives with relatively better performance are mentioned here (Fig. 1). Computational modelling suggests that such heterocyclic rings modify the electronic distribution and steric assembly of the DCF core. Incorporating heteroatoms (O, S, and N) enhances H-bonding and molecular interactions with the COX enzyme, potentially enhancing anti-inflammatory effects. *In silico* docking and ADMET prediction also suggest that such substitutions can enhance lipophilicity, absorption, and metabolic stability. Additionally, changes to R_1 and R_2 could prevent the generation of toxic metabolites known for DCF toxicity. Thus, computationally designed DCF analogues that incorporate these heterocycles may show enhanced binding affinity and better pharmacokinetic properties, as well as potentially reduce the toxicity.

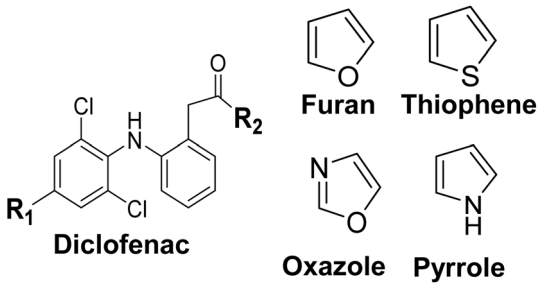

Fig. 1 Structural details of DCF with R_1 and R_2 positions.

2. Materials and methods

2.1. Geometry optimization

Computational approaches are increasingly utilized in the pharmaceutical sector to enhance the understanding of innovative drug features. As a result of computational approaches' improved ability to predict the behavior of previously unknown molecules, their adoption has skyrocketed in the pharmaceutical industry. The drug development process often makes use of computational techniques to predict the medicinal potential of new chemicals. The source of DCF was PubChem (https://pubchem.ncbi.nlm.nih.gov/), a web-based database of chemical structures (PubChem CID: 3033). The optimization of DCF's geometry and structural alteration, together with all quantum chemical computations of the newly created analogs, were carried out using Gaussian 16. Optimizing the geometry and structural alteration of DCF and performing all computational calculations of the newly discovered analogs were both

accomplished using Gaussian 16. The Gabedit software was utilized to analyze molecular dynamics and structural alterations to ascertain a relatively robust and energetically favorable conformation by employing the projected assisted model building with energy refinement (AMBER) estimated value. Molecular geometry optimization in the gas phase was accomplished by means of density functional theory (DFT), B3LYP, and 6-31G+(d,p) as basis set. Through the use of time-dependent density functional theory (TD-DFT), the electronic transitions of these molecules were examined. The properties of the frontier molecular orbitals were determined by calculating the HOMO and LUMO, or the highest occupied and lowest unoccupied molecular orbitals, respectively. The recognized equations were used to determine the HOMO–LUMO energy gap, hardness (η), softness (S), potentiality (μ), electronegativity (χ), and electrophilicity (ω).[25]

2.2. Molecular docking and interactions calculation

The three-dimensional crystal structure of human cyclooxygenase-2 (prostaglandin-endoperoxide synthase-2, PDB ID: 5IKR) was obtained from the RCSB Protein Data Bank (https://www.rcsb.org/). Before docking, the crystallographic water molecules, heteroatoms, co-crystallized ligands, and superfluous chains were removed from the protein by employing PyMOL (v1.7.4) and BIOVIA Discovery Studio 2021. By adding missing hydrogen atoms and energy minimizing the structure with Swiss-PdbViewer (v4.1.0), steric conflicts were eliminated and geometry optimized. COX-2's active site was determined by the binding pocket of DCF and other inhibitors, the co-crystallized ligand coordinates, and previously published structural data. AutoDock Vina was used to dock geometry-optimized DCF analogues into the improved COX-2 binding site, utilizing the PyRx (v0.8) virtual screening interface. Flexible ligands were allowed because the protein was a stiff macromolecule. A three-dimensional grid box centered on the catalytic pocket encompassed the empirically identified active site (Fig. S5). The binding cavity was covered with computationally efficient grid dimensions. Multiple binding poses were generated for every single ligand, and the conformation exhibiting the minimal predicted interacting free energy (optimal Vina score) and appropriate active site orientation was chosen for analysis. BIOVIA Discovery Studio 2021 and PyMOL (v3.1) visualized COX-2's non-covalent interactions with docked ligands. Hydrogen bonds, hydrophobic contacts, pi–pi stacking, cation-pi interactions, and other intermolecular forces were examined in two-dimensional interaction diagrams and three-dimensional structural views to determine binding determinants. The docking profiles were cross-checked and visually evaluated to ensure that the ligands occupied the canonical COX-2 channel and maintained chemically acceptable interactions. Docking and interaction profiles were employed to compare DCF and its developed derivatives' COX-2 active site binding.

2.3. Molecular dynamics (MD) simulation

Molecular dynamics (MD) simulations were performed for the three primary analogues (DCF2, DCF4, and DCF6) alongside the progenitor DCF, each in association with the protein structure (PDB ID: 5IKR), utilizing YASARA Dynamics with the AMBER14 force field.[26] MD simulation has been performed for only 3 top docking analogues (DCF2, DCF4, and DCF6), as well as the parent DCF, which were selected based on their best docking score with active-site key residues (Fig. 6 and Table S6) and reasonable ADMET predicted data (Table 1). All these compounds showed low docking scores during the docking study, which indicates a higher probability for stable complex formation with the target protein. A thorough cleaning and optimization of the docked complexes was performed before simulation, ensuring that the H-bonds were correctly oriented. The complexes were solubilized utilizing the TIP3P water model through periodic boundary conditions. The temperature was adjusted to 298 K, the pH to 7.4, and the concentration of NaCl was adjusted to 0.9%. The steepest gradient method was used to perform primary energy minimizations in 5000 cycles using the simulated annealing techniques.[25] The estimation of electrostatic interactions over long distances was assessed using the Particle Mesh Ewald (PME) method and a threshold radius of 8.0 Å and a time period of 2 fs.[27] Over the course of 100 ns, the Berendsen thermostat maintained a steady temperature and pressure for the simulations. Each

Table 1 ADMET prediction of some selected DCF analogs[a]

	Absorption					Distribution		Metabolism	Toxicity				
Name	BBB	HIA	C2P	P-GpI	ROCT	BBB	P-GpI	CYP2C9 inhibitor	HER GI	AMEST	NC	BD	AOT
DCF	0.954	0.954	0.886	0.825	0.908	0.650	0.258	0.694	0.951	0.913	0.671	0.972	0.760
DCF1	0.975	0.990	0.681	0.894	0.889	0.484	0.660	0.876	0.981	0.899	0.735	1.000	0.631
DCF2	0.954	0.992	0.655	0.781	0.903	0.522	0.648	0.669	0.967	0.896	0.694	0.981	0.551
DCF3	0.957	0.989	0.677	0.815	0.908	0.522	0.648	0.709	0.989	0.833	0.702	0.991	0.669
DCF4	0.948	0.987	0.537	0.927	0.945	0.480	0.511	0.000	0.993	0.907	0.784	1.000	0.528
DCF5	0.994	0.975	0.574	0.655	0.665	0.750	0.640	0.949	0.881	0.636	0.786	1.000	0.609
DCF6	0.994	0.994	0.711	0.546	0.771	0.846	0.559	0.932	0.893	0.544	0.481	0.964	0.540
DCF7	0.992	0.992	0.669	0.739	0.746	0.831	0.668	0.866	0.928	0.735	0.732	0.978	0.507
DCF8	0.996	0.995	0.610	0.787	0.815	0.816	0.368	0.896	0.931	0.827	0.807	1.000	0.627

[a] BBB = blood–brain barrier, HIA = human intestinal absorption, C2P = Caco-2 permeability, P-GpI = P-glycoprotein inhibitor, ROCT = renal organic cation transporter, HERGI = human ether-a-go–go-related gene inhibition, AMEST = AMES toxicity, AOT = acute oral toxicity, NC = non-carcinogenic, BD = biodegradation, AOT = acute CYP2C9Oral toxicity.

system (DCF2, DCF4, and DCF6) was solvated in a periodic simulation box with a minimum distance of 10 Å between the solute and the box boundary, ensuring sufficient solvent coverage and minimizing artificial interactions across periodic boundaries. A single simulation run was conducted for each system. Trajectories were recorded every 100 ps and subsequently analyzed to evaluate root mean square deviations (RMSD), hydrogen bonding, radius of gyration (R_g), solvent-accessible surface area (SASA), and root mean square fluctuations (RMSF).[25]

2.4. ADMET and PASS prediction

The drug's absorption, distribution, metabolism, excretion, and toxicity (ADMET) profile has a significant impact on therapeutic efficacy. ADMET characteristics of a compound are integral to its pharmacological activity. Drug pharmacokinetics, which comprises uptake or absorption into the bloodstream, distribution to target tissues, metabolism, excretion or elimination, and toxicity, all affect the therapeutic outcome. The producing system used in all cases SMILES with other structured files. The ADMET study, in particular, has a significant impact on a drug's availability and metabolism, its half-life as well as its level of toxicity, and is therefore key to the optimal therapeutic effect. The prediction of ADMET information relies on the AdmetSAR server (https://lmmd.ecust.edu.cn/admetsar1).[28] The PASS prediction server (https://www.way2drug.com/passonline/) offers access to precise measurements concerning the bioactivity range, aimed at identifying the characteristics of bioactive compounds.[29]

3. Result and discussion

3.1. Thermodynamic analysis

Thermodynamic characteristics, including enthalpy, Gibbs free energy change, and electronic energy of a chemical, are regarded as dependable indicators of stability, reactivity, and interaction.[25,30] These parameters are a measure of the overall energy balance for a molecule and indicate whether a chemical change due to reaction is endothermic or exothermic. Stability, from the thermodynamic point of view, is affected by structural alterations in terms of enthalpy and free energy.[26] The enthalpy, dipole moment, electrostatic potential, and binding energy may vary significantly with slight structural variations of the molecule.[25]

Fig. 2a and Table S2 show the calculated Gibbs free energies (Hartree) of DCF and its analogues. DCF has the maximum energy (−1665.60 hartree), indicating the least thermodynamically stable moiety. On the other hand, DCF2 (−2217.37 hartree) and DCF3 (−2217.37 hartree) showed the most negative values of Gibbs free energies, which are the highest among all calculated values, indicating them as significantly more stabilized than DCF. The other analogues, DCF1 (−1874.52 hartree), DCF4 (−1910.45 hartree), DCF5 (−1799.28 hartree), DCF6 (−1819.15 hartree), and DCF8 (−1835.20 hartree), have intermediate energy compared to that of the respective more stable counterparts and tend to be highly stabilized due to structural modification (Table S2). This indicates that most chemical modifications do not seek to destabilize the DCF core, but in fact, they usually diminish the total energy of the complex and therefore increase its thermodynamic stability. All the structurally modified DCF analogues exhibit reduced energy than DCF due to the introduction of selective electron-donating or withdrawing groups within the analogues, and thus indicate enhanced chemical reactivity (Table S2).

The polarity and possible interaction profile of DCF and its derivatives are further illuminated by the dipole moment (Fig. 2b). The dipole moment of the parent DCF is comparatively low (2.36 debye), indicating minimal overall polarity. Moderate dipole moments in NSAIDs and related compounds result in the desired balance of hydrophobic/electrostatic interactions at the active site of the enzyme, thus assisting an efficient association with optimal pharmacokinetic characteristics.[31,32] In particular, dipole moments of DCF2, DCF4, DCF6, DCF7, and DCF8 are all larger than that of the parent drug (DCF) (Table S2), meaning they could potentially interact more strongly with polar residues in COX-2 or other off-target proteins to cause changes in potency or selectivity. Moderate increases in polarity may enhance dipole–dipole or ion–dipole interactions with polar residues in the COX-2 active site or adjacent binding areas.[25,31] Simultaneously, these values remain within a range that likely maintains

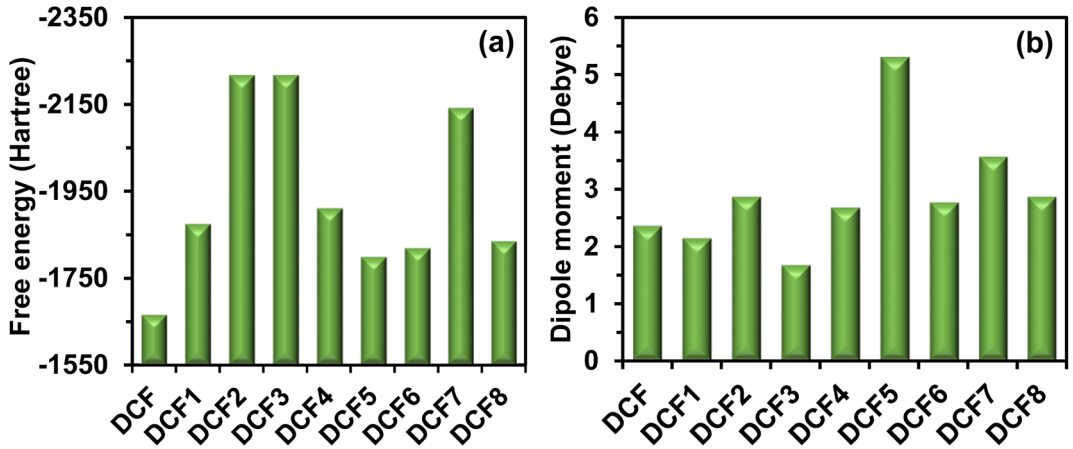

Fig. 2 (a) Free energy, and (b) dipole moment of the DCF and its derivatives.

sufficient lipophilicity for membrane penetration and systemic dispersion. As a result, these derivatives may attain an improved equilibrium among solubility, target affinity, and pharmacokinetic properties. On the contrary, the remarkably high dipole moment of DCF5 (5.31 debye) indicates that it is highly polar. Although this may improve aqueous solubility and facilitate robust electrostatic interactions with polar amino acids, excessive polarity could hinder passive diffusion across biological membranes and consequently elevate metabolic clearance. Such features may adversely impact bioavailability, despite promising interaction potential at the protein level.[33,34] DCF1 and DCF3 are the least polar amongst all other molecules (a dipole moment of 2.15 and 1.68 debye, respectively). Thermochemical investigation reveals that, when compared with DCF, most of the new derivatives exhibit higher thermodynamic stability and modified polarity profiles. Reduced polarity may increase membrane permeability but can diminish electrostatic interactions with polar residues in protein binding sites. DCF2, DCF7, and DCF8 may be considered for the promising candidates, integrating the significant energy stabilization, having medium dipole moments, and thus exhibiting the improved docking score as well as the ADMET profile.[25,27]

The total heat content of any molecule is represented by enthalpy, which is also related to the bond strength and the overall stability of any molecule.[35] Usually, compounds with lower enthalpy values correspond to more stable compounds. DCF (−1665.53 hartree) and all of its derivatives possess negative enthalpy values, indicating that these compounds release energy when they combine with others (Table S2). Among the derivatives, DCF2 and DCF3 possess the lowest enthalpy of −2217.29 and −2217.30 hartree, respectively. DCF1, DCF5, DCF6, and DCF8 have the higher enthalpy values of −1874.45, −1799.20, −1819.08, and −1835.12 hartree, respectively. Therefore, DCF2 and DCF3 are thermodynamically favored and exhibit greater thermodynamic stability with the lowest values in both Gibbs free energy and enthalpy.

3.2. Frontier molecular orbital analysis

The frontier molecular orbitals (FMOs) indicate the reactivity and kinetic stability of any molecule based on the energy difference between HOMO and LUMO, which reveals the charge transfer, excitation, and intermolecular interaction.[36] Koopman's theorem and the concept of conceptual DFT imply that the energy level of HOMO is approximately relevant to the ionization potential (affinity for removing electrons) and LUMO with electron affinity (affinity for absorbing electrons). The minor energy gap correlates with significant chemical reactivity and elevated kinetic stability, or hardness, which typically

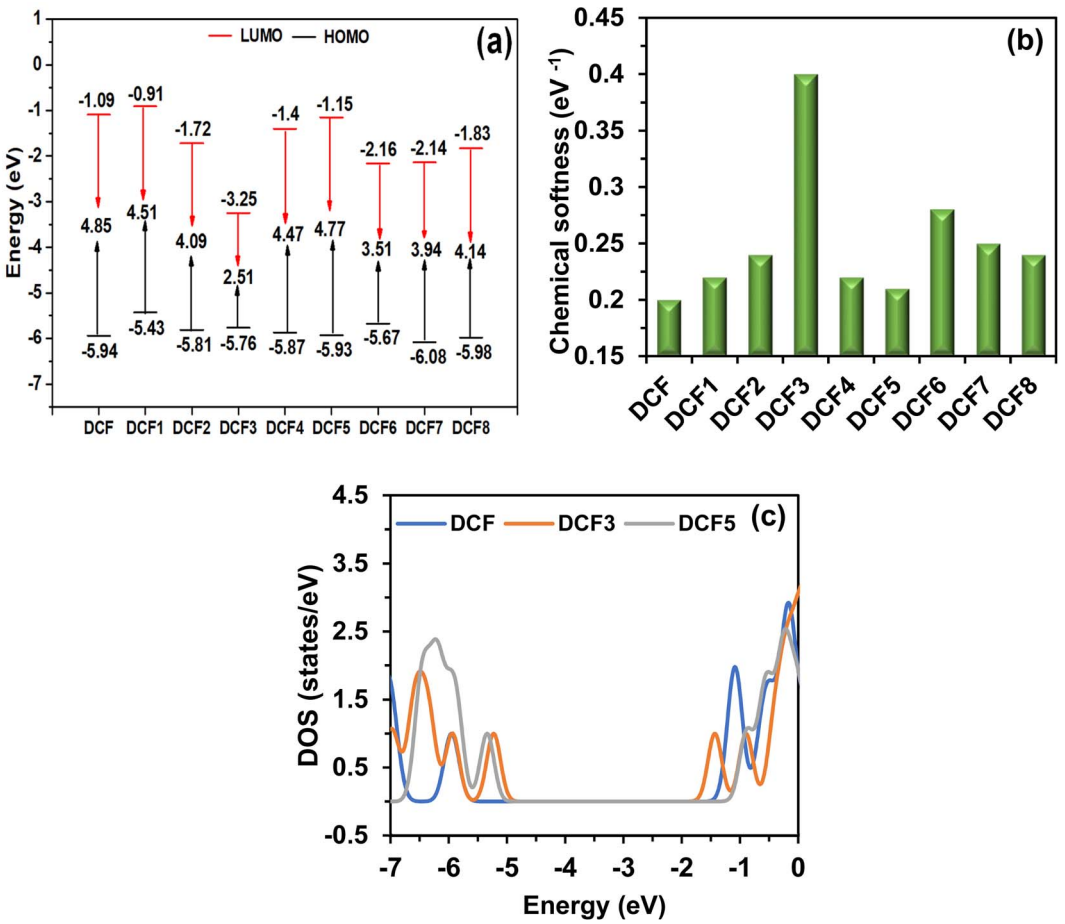

Fig. 3 (a) HOMO–LUMO energy gap, (b) softness, and (c) DOS plot of DCF and its derivatives.

associates with a greater energy gap when overlapping with a higher energy gap.[37] DCF has HOMO and LUMO values of −5.94 eV and −1.09 eV, with a bandgap energy of 4.85 eV, respectively (Fig. 3a, S2 and Table S3). On the other hand, DCF3 possesses a much smaller energy gap of around 2.51 eV (LUMO = −3.25 eV, HOMO = −5.76 eV), demonstrating that the stability state predicted for its LUMO is possibly a result of further π-conjugation and powerful electron-donating substituents. The energy gaps of the derivatives (DCF6 = 3.51 eV and DCF7 = 3.94 eV) have significantly lower values compared to DCF, indicating enhanced softness and polarizability. Under ideal structural and stereochemical conditions, DCF3, DCF6, and DCF7 are expected to exhibit improved reactivity or target engagement due to the mechanistic relationship between a narrower HOMO–LUMO gap and increased chemical reactivity, as well as the possibility of intermolecular charge transfer. On the other hand, for larger energy gap derivatives (DCF1 = 4.51 eV, DCF4 = 4.47 eV, and DCF5 = 4.77 eV), better kinetic stability or less off-target reactivity could be offered.

Chemical softness denotes the facilitation of charge transfer within a molecule and acts as an indicator of molecular reactivity and polarizability; more softness correlates with a greater propensity for the molecule to modify its electronic cloud in response to external disturbances.[38] The chemical softness values of DCF and its derivatives vary significantly, ranging from approximately 0.20 eV to 0.40 eV, which is a result of electronic changes in the modified structures (Fig. 3b). The softness value of the DCF is approximately 0.20 eV, which indicates that it is moderately reactive, chemically and thermodynamically stable. Among all the derivatives, DCF3 exhibits the most chemical softness, with a value of around 0.40 eV, which is in line with its lowest HOMO–LUMO energy gap of 2.51 eV. DCF3 exhibits superior polarizability and reactivity, and is effective for intermolecular charge transfer as well as increased biological activity. Due to structural modification, DCF3 may insert strong substituent groups or remove electrons, which results in enhanced softness and reduced energy gaps.[39] DCF4 and DCF5, on the other hand, are comparably slightly less soft (0.22 eV and 0.21 eV), which is in line with their wider energy gaps (4.47 and 4.77 eV). This is indicative of higher chemical hardness and, thereby, greater molecular stability. In addition, DCF6 is very soft (0.28 eV) and has a further lower-lying gap of 3.51 eV, balancing reactivity and stability. DCF3 and DCF6 are more flexible than others, suggesting that they would have a corresponding better ability to transfer electronelectrons, which should make stronger binding between them and biological macromolecules such as the COX-2 binding pocket. Such a result is consistent with other computer-aided drug design (CADD) studies on the DCF derivatives.[25,27] The DOS plot illustrates the distribution of electronic states at different energies and is plotted near the Fermi level (Fig. 3c). DCF, DCF3, and DCF5 demonstrate the direct influence of the other orbital contributions on electronic transitions and charge mobilities in these molecules. With reduced electrical mobility and a smaller DOS in the low-energy region, DCF5 exhibits decreased reactivity. The similarity of the density of states between DCF and DCF5 also emphasizes their similar electronic hardness, which ensures long-term stability.

3.3. Molecular electrostatic potential

Charge distribution changes caused by various functional groups and substituents have been shown using molecular electrostatic potential (MEP) maps of DCF and its derivatives, thereby predicting how electron-donating and electron-withdrawing groups could modify reactivity and potential interactions with biological targets (Fig. 4 and S3).

DCF has a charge density of $\pm 5.843 \times 10^{-2}$ and has both a carboxyl group (–COOH) and an amine group (–NH_2). The carboxyl group pulls all the electrons in the molecule toward itself because it attracts them. This makes the region around the oxygen atoms exceedingly negative. Because this structure has a negative charge, DCF is a nucleophile and a good hydrogen bond acceptor. The amine group sends out electrons, which generates a positive potential around the hydrogen atoms. The electron density around the DCF1, DCF2, DCF5, and DCF6 molecules varies a lot based on the groups that are attached to them (Fig. 4 and S3).

There are halogen atoms (Cl) or sulfonyl groups (–NH_2) in DCF5 and DCF6. The molecule gives electrons to both groups. These substituents also make the MEP map show more negative potential values by reducing the electron density around the

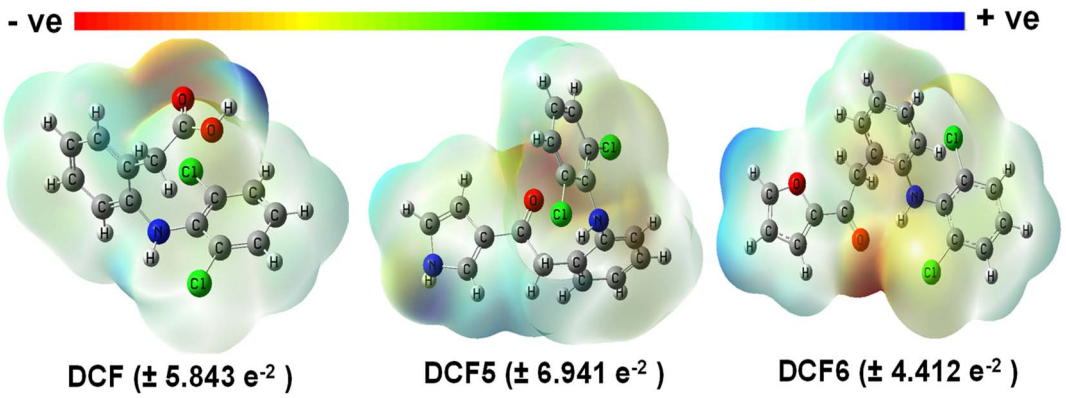

Fig. 4 MEP map of DCF and some of its derivatives.

carboxyl group. The MEP map reveals that DCF1 and DCF2, which have groups that give electrons like methoxy or alkyl, have a less negative potential. These groups provide the molecule electrons, which makes it more stable by making the area around the amine and hydroxyl groups more dense with electrons. They also add more sections that are neutral or slightly negative to the DCF, which makes it less lacking in electrons.

3.4. FT-IR spectral analysis

This study conducted spectral characterization, which was subsequently compared with the experimental data of the parent drug DCF (Table S4). In this study, the FT-IR spectral vibrational frequencies are computed within the 500–4000 cm^{-1} range to validate the presence of the desired functional groups for DCF and its analogues (Fig. 5a and S4). The data were subsequently corrected by applying a scale factor of 0.9688 to enhance accuracy (Table S4). Asymmetrical stretching of aromatic C–H bonds is detected from 3065 cm^{-1} to 3098 cm^{-1}, whereas from 3000 cm^{-1} to 3100 cm^{-1} in experimental FT-IR. In experimental FT-IR, the N–H bond was shown to stretch at 3346 cm^{-1} to 3584 cm^{-1}, and in experimental FT-IR, it was 3300–3500 cm^{-1}. Furthermore, stretching of aromatic C=C is observed at 1550 cm^{-1} to 1597 cm^{-1}, whereas 1450 cm^{-1} to 1600 cm^{-1} in experimental data and 1653 cm^{-1} to 1762 cm^{-1} frequency is indicated for C=O, which is in good agreement with real data 1690 cm^{-1} to 1720 cm^{-1} as shown in Fig. 5a. The difference in the stretching frequency position for each was discovered regarding the structural modification of the DCF at different sites employing distinct functional groups in addition, the aromatic C=C stretching is detected between 1550 and 1597 cm^{-1}, whereas the experimental data shows a range of 1450 to 1600 cm^{-1} and a range of 1653 to 1762 cm^{-1} for C=O, which roughly corresponds to the range of 1690 to 1720 cm^{-1} shown in Fig. 5a. Various functional groups were used to modify the DCF structurally at different places, and it was found that the stretching frequency position varied for each case.

3.5. UV-visible spectral analysis

Fig. 5b shows the UV-visible spectra of DCF and its derivatives, which enable us to comprehend the electronic transitions and conjugation effects in the surrounding molecular orbitals. The DCF also exhibits a strong absorption band at 284 nm (excitation energy = 4.35 eV), originating from $\pi \rightarrow \pi^*$ transitions of its aromatic ring system and $n \rightarrow \pi^*$ transitions localized on the carbonylic carbonyl group (Table S5). This peak at 284 nm is a signature feature of DCF, and the change from the ground state (S_0) to the first stimulated state (S_1) is reflected in it, associated with the HOMO → LUMO (H → L) transition, contributing 82.90% to the transition with an oscillator strength of 0.0499.

The intensity of the molecular interaction driving the transition is reflected in this percentage of configuration. This H → L transition clearly demonstrates that DCF has a robust electronic structure capable of readily absorbing UV light at 284 nm, which is significant for its UV-Vis characterization, since it occurs frequently. Derivatives' shifting absorption maxima reveal how their electrical properties are impacted by structural alterations.[40] For the H → L transition, DCF1 exhibits a configuration percentage of 90.14%, a redshift of 795 nm, and an excitation energy of 1.56 eV (Table S5). But compared to DCF, its oscillator strength is smaller at 0.0173. Similarly, for the H → L transition, DCF2 (472 nm) and DCF3 (342 nm) exhibit configuration percentages of 97.35% and 97.31%, respectively, with oscillator strengths of 0.0038 and 0.4817, respectively. Because of its structural alteration, DCF3 exhibits the strongest electronic excitation of the derivatives, as evidenced by its high intensity. Substituents that remove electrons or give them resonance cause the red-shifted readings in DCF1 (795 nm) and DCF2 (472 nm) to indicate that π-conjugation persists for

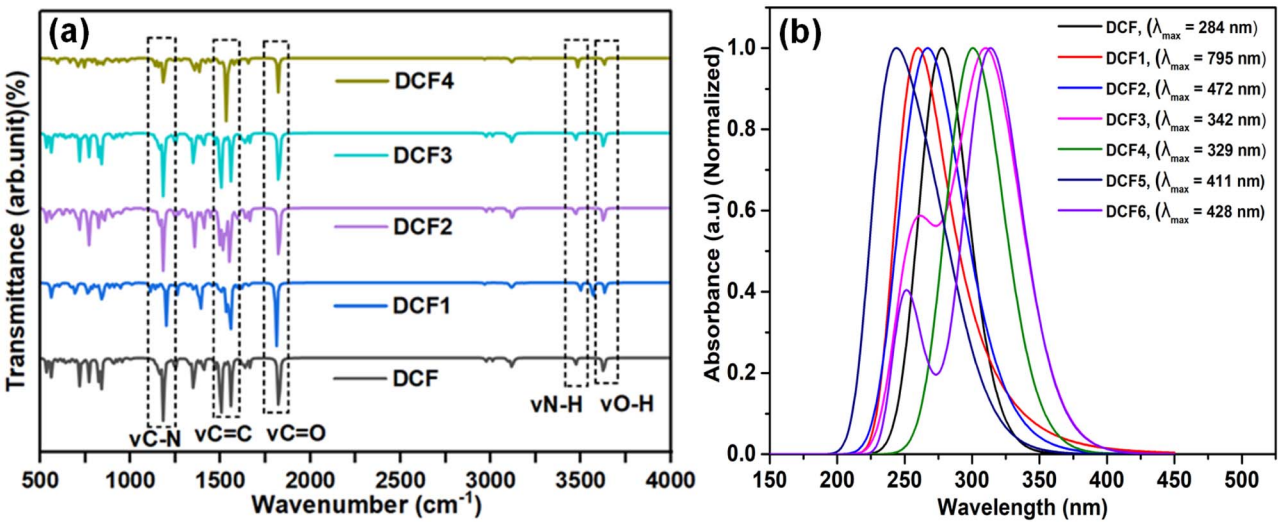

Fig. 5 (a) FT-IR and (b) UV-Vis spectra of DCF and its derivatives.

a longer period and that the HOMO–LUMO energy gaps decrease. In addition, DCF4 (329 nm), DCF5 (411 nm), and DCF6 (428 nm) all exhibit robust H → L transitions associated with varying excitation energies and oscillator intensities. Despite having smaller oscillator strengths, DCF4, DCF5, and DCF6 all show robust H → L transitions with configuration percentages of 96.87%, 88.36%, and 97.79%, respectively. Despite the weaker oscillator powers, all of these exhibit significant H → L transitions. DCF3 and DCF4 only show modest red shifts in comparison to the DCF, indicating weaker substituent effects or a limited conjugation extension. Relative intensities and peak broadening across the sequence also show variations in electron cloud movement and oscillator strength. DCF7, with a contribution of 94.42%, also exhibits a strong H → L transition, but the slight decrease compared to DCF8 indicates that its structural modifications may have caused a less favorable electronic configuration or a more localized transition. The oscillator strength of DCF7 (0.0816) is higher than that of DCF8 (0.0004), further suggesting that while the electronic excitation is strong in DCF7, the efficiency of the transition in DCF8 is more pronounced due to a larger contribution of the H → L transition.

3.6. Molecular docking: binding affinity and analysis of nonbonding interactions

Molecular docking constitutes a fundamental technique within the discipline of CADD, facilitating the prediction of binding preference and the chemical interactions occurring between a ligand (drug) and its corresponding receptor proteins.[41,42] This structure-based technique facilitates the computational investigation of compounds and is instrumental in defining the spatial positioning, orientations, and conformations of ligand three-dimensional structures within macromolecules.[43] In molecular docking, the greater negative value signifies stronger binding between proteins and receptors.[25] In our study, DCF and all of its analogues have shown strong binding with 5IKR (Fig. 6 and Table S7). Although all of the analogues exhibited higher binding affinities, DCF's is −6.6 kcal mol^{-1}. DCF3 shows the most significant at −7.5 kcal mol^{-1}, followed by DCF2 at −7.3 kcal mol^{-1}, DCF1 at −7.1 kcal mol^{-1}, DCF2 at −7.3 kcal mol^{-1}, DCF7 at −7.3 kcal mol^{-1}, and DCF8 at −7.2 kcal mol^{-1}. DCF4 and DCF5 had a slightly reduced binding affinity of −7.0 kcal mol^{-1} and 6.9 kcal mol^{-1}. Although the highest binding score was reported by DCF3, which is −7.5 kcal mol^{-1}, its binding site was different compared to DCF and its other derivatives. Comparing DCF3, it appears that structural and physicochemical modifications resulted in a distinct binding pocket. Steric strain from bulkier substituents may prevent the molecule from fitting into the narrow COX catalytic channel, where DCF generally interacts. Moreover, larger molecular sizes or extra functional groups may introduce more H-bonds or hydrophobic interactions in the protein's alternate cavities. Additionally, polarity or electronic distribution alterations may increase affinity for residues outside the conventional active site. There may be limits to molecular docking, such as the rigid protein assumption, which might lead to larger or different ligands being steered to energetically favorable non-catalytic locations. All of these considerations can explain why DCF3 may have a lower docking score, even if it binds in a different pocket.

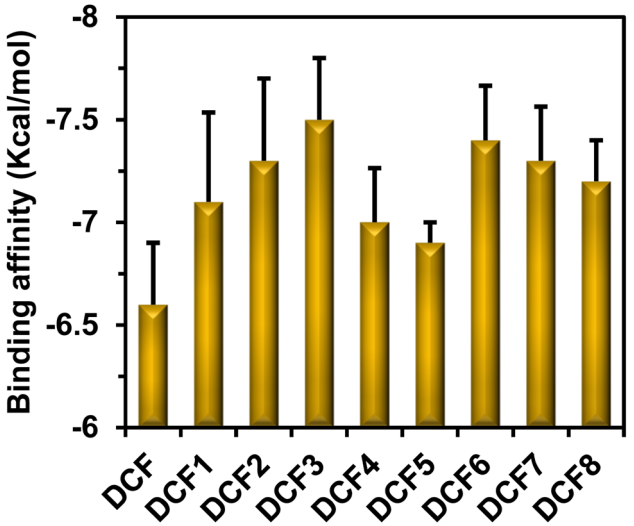

Fig. 6 Binding affinity of DCF and its derivatives with COX2α (PDB ID: 5KIR), representing potential for targeted inhibition.

Both the H-bond donor (shown by pink) and the H-bond acceptor (represented by green) rely on the H-bond in nonbonding interactions (Fig. 7). H-bonds formation, as well as C–H bonds, and hydrophobic bonds stabilize the docking structure, and these non-covalent interactions influence the binding affinity and overall drug effectiveness.[26] The dimensions (Angstrom) of the grid box for site-specific docking in PyRx are *X*: 76.15, *Y*: 60.46, and *Z*: 64.03, respectively (Fig. S5). An increase in the binding affinity of ligands and receptors may be caused by H-bonding at a position less than 2.3 Å.[27] Common amino acid residues that interact with most of the variants are ARG120, TYR115, VAL89, ILE112, and LEU93.

These interactions mostly demonstrated the existence of typical H-bonds, π–π T-shaped contacts, and π-alkyl interactions (Table S6). The majority of the analogues established typical H-bonds with amino acid residues, including ARG120, TYR355, THR212, GLU465, SER119, and GLY135, with bond distances ranging between 2.1 and 2.9 Å. A typical H-bond consists of a hydrogen atom covalently bonded to a strongly electronegative donor atom, accompanied by an electrostatic interaction with an acceptor atom. They are considered primary stabilizing forces for protein–ligand complexes with strong binding affinity.[44] Almost all analogues formed Pi-alkyl bonds, and some of them were treated with VAL89, ILE112, VAL291, PRO153, and LEU93, which contribute to enhancing the stability and improving the hydrophobic interactions of the ligand (drug) in the active site of the receptor.[45] Additionally, carbon-hydrogen bonds, π-cations, π-anions, and π-sigma bonds were observed in some compounds.

Despite DCF3 having quantum-chemical characteristics that are extremely beneficial in terms of thermodynamic stability, lower HOMO–LUMO gap, and higher softness, this data does

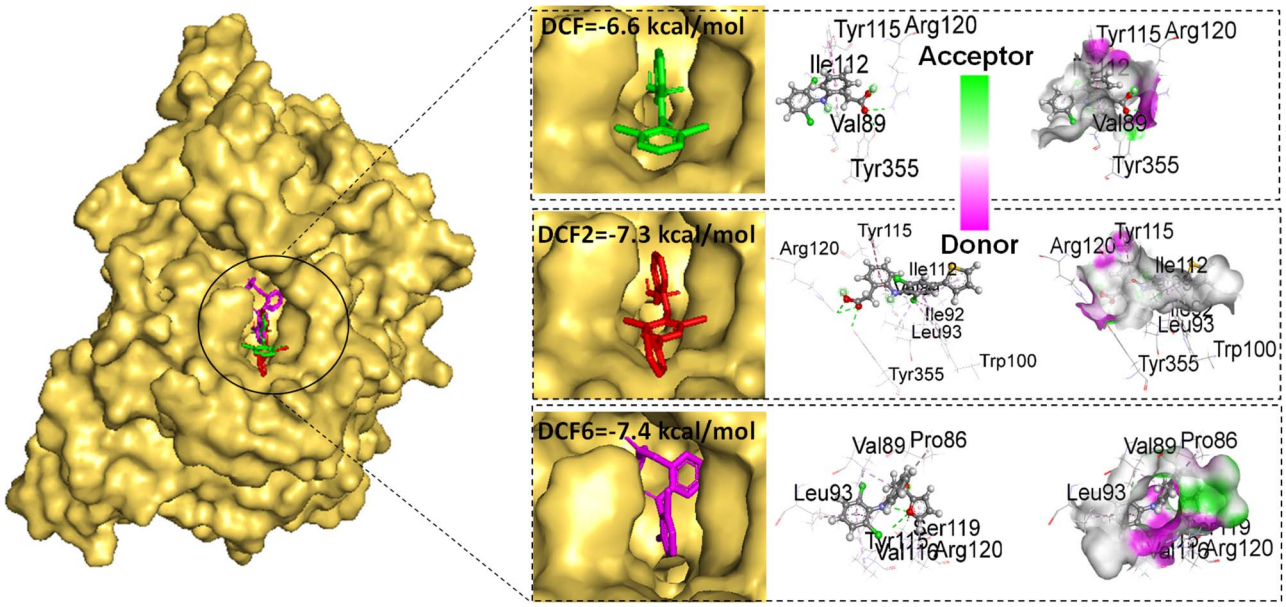

Fig. 7 DCF's receptor protein active sites selected by superimposed docked conformers, nonbonding interactions, and H-bond surface area with receptor protein (5IKR).

not directly imply biological significance. Notably, DCF3 accommodates a non-conventional binding mode, suggesting that it would not be the best candidate for a classical COX-2 inhibitor. In comparison, DCF2, DCF4, and DCF6 show more stable binding in the canonical active site with less toxicity as well as better molecular dynamics behavior and reasonable ADMET profiles. Therefore, these compounds are considered more suitable candidates for further development despite the comparatively superior intrinsic electronic properties of DCF3. Such non-canonical binding may lead to reduced potency in relevant functional assays, where the classic active site is an important aspect for the intended therapeutic effect. DCF3 binds to off-targets or pocket which are discordant with the canonical enzymatic function, leading to loss of COX-2 inhibitory effect or diminished drug modulation of inflammatory pathways. Moreover, this binding could potentially enhance the potential for off-target effects due to DCF3's ability to bind undesired enzymes or receptors that possess analogous moieties, similar to how antidepressants do. Additionally, binding in a non-canonical pocket could impact the pharmacokinetic properties of DCF3, including absorption, distribution, metabolism, and excretion (ADME). This altered binding may change the drug's solubility, bioavailability, and target tissue penetration. Specifically, changes in binding might impact the metabolism of DCF3 or its ability to traverse the BBB, with potential effects on CNS side effects.

3.7. Molecular dynamics simulation

To validate the docking poses as well as assess the dynamic stability of the complexes, 100 ns all-atom MD simulations were conducted with 5IKR involving the parent drug DCF and its top three analogs (DCF2, DCF4, and DCF6). The trajectories were examined using the following metrics: RMSD, RMSF, R_g, total number of intermolecular H-bonds (Fig. 8a–d) and (SASA) (Fig. S6).

The RMSD profiles of all four complexes (DCF, DCF2, DCF4, and DCF6) swiftly converged during the initial few nanoseconds, and subsequently oscillated within a limited range throughout the duration of the simulation (Fig. 8a). The highest and smallest RMSD values for DCF, DCF2, DCF4, and DCF6 are 2.478 Å, 2.907 Å, 2.185 Å, 2.738 Å and 0.408 Å, 0.374 Å, 0.403 Å, and 0.38 Å, respectively. The complexes primarily oscillated between 1.2 and 2.5 Å following initial equilibration, suggesting that there was no notable structural drift or unfolding of 5IKR over the 100 ns dynamic simulation period. The mean RMSD values for the DCF, DCF2, DCF4, and DCF6 complexes were 1.78 $\pm$ 0.320, 1.901 $\pm$ 0.319, 1.573 $\pm$ 0.263, and 1.759 $\pm$ 0.292. For DCF2, the RMSD slightly increases at approximately 10 ns and 90 ns, while for DCF6, it reaches values close to 3.0 Å at approximately 40 ns and 90 ns. However, this change was a transitory one and produced no enduring effect on the molecule's conformation. The plateau of RMSD is steady, which suggests that the four ligands held their initial binding poses in 5IKR. The complexes' RMSF results show the flexibility of the amino acid residues. The per-residue RMSF was highly comparable between complexes, and even in the case of the different types of simulated complexes. The findings indicate that all four analogs stayed stable in the original binding sites as no alteration was observed during 100 ns MD simulations. The residue-specific RMSF (Fig. 8b) demonstrates that most amino acids deviate only a small fraction, as expected for a well-folded and stiff protein core. Especially, the RMSF values of flexible and solvent-exposed loops and terminal segments are high. The smaller RMSF values of DCF6 compared with DCF reflect a more stable protein structure in the complex. The

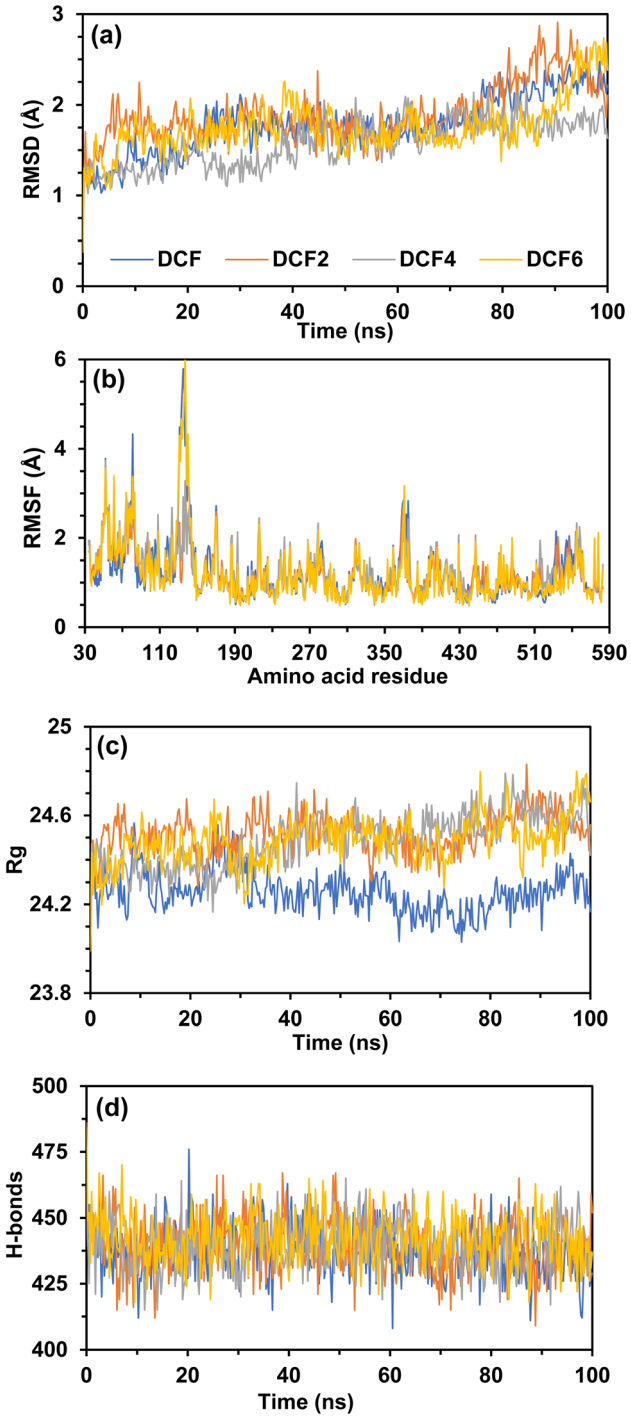

Fig. 8 Molecular dynamics simulation of the top four DCF-5IKR complexes over 100 ns in terms of (a) RMSD, (b) RMSF, (c) R_g, and (d) total number of H-bonds.

presence of a ligand is manifested in an R_g value and the extent of complex mobility. More conformational stability is suggested by a lower R_g value, whereas more flexibility is indicated by a higher R_g value. DCF showed the minimum R_g value, and in specific amino acid residues, DCF4 and DCF6 also had lower R_g values, suggesting that all of the analogues formed a tight and stiff complex with 5IKR (Fig. 8c). An additional analysis was conducted utilizing the amount of intermolecular bonds produced in the complexes to further improve comprehension of structural stability.

The stability of protein structures is dependent on hydrogen bonding. The average number of hydrogen bonds detected in 5IKR and its complexes with DCF, DCF2, DCF4, and DCF6 was 437.93, 439.92, 439.88, and 442.38, respectively (Fig. 8d). The 5IKR-DCF complex had the fewest hydrogen bonds, while the 5IKR-DCF2 complex had the maximum number. A change in the extent of the surface of the protein complexes was measured using the SASA. Higher SASA values suggest an expansion in protein volume, whereas lower SASA values correspond to a truncated protein conformation. (Fig. S6) indicates that all four complexes had stable SASA profiles, but the higher SASA values of DCF6 might be the reason behind the expansion of their surface area, likely resulting from structural folding or unfolding transitions during the simulation. The MD simulation results demonstrate that DCF and its three selected analogs form dynamically stable complexes with 5IKR. The limited RMSD and RMSF values, nearly constant R_g and SASA profiles, and preserved H-bond network collectively indicate that the ligand interaction does not disrupt the overall conformation of 5IKR, and the docked postures maintain stability across the 100 ns timescale. Among these, the behavior of DCF6 is in good agreement with its favorable binding free energy, supporting its designation as a highly prospective option, DCF-based derivatives for further optimization and experimental validation.

3.8. ADMET analysis

A combined *in silico* evaluation of ADMET properties was performed to predict the pharmacokinetics and safety of DCF and its selected analogs (DCF1–DCF8) (Table 1). Such computational estimates prove to be essential during the initial stages of drug development because they help to determine, before evaluation of *in vitro* or *in vivo* validation on the compound, whether it has good absorption, metabolic stability, and low toxicity.[46] The potential of oral bioavailability was also quantified by testing the following aspects of absorption: blood–brain barrier permeability (BBB), human intestinal absorption (HIA), Caco-2 permeability (C2P), P-glycoprotein inhibition (P-GpI), and renal organic cation Transporter (ROCT). In ADMET prediction, the threshold is considered to be 1.00 for all the indices/parameters mentioned in Table 1.

The BBB permeability values (0.948–0.996) of all drugs were large, and as a result, indicated that they had the potential to reach the CNS. While this can enhance the therapeutic effect in treating CNS inflammation, it also raises the risk of central nervous system adverse effects, such as dizziness, sedation, cognitive impairment, seizures, or even neurotoxicity. Therefore, clinical care is essential to monitor and mitigate these potential risks while maximizing the therapeutic benefits. The HIA values (0.954–0.995) of all the analogs in the case of oral dose were extremely high, which implies that they are absorbed by intestinal epithelia. In the range of C2P (0.537 to 0.886), moderate to high values of membrane permeability are observed. C2P of DCF and DCF8 was most effective, and this

implies that they were transported to the intestinal lumen with ease. Most of the analogs inhibit P-glycoprotein significantly, especially in DCF4 and DCF5, as it is shown by 0.546–0.927 of P-GpI. The ROCT values varied from 0.665 to 0.945, signifying that the analogs are effectively excreted by the kidney with minimal accumulation, which would not result in significant renal cation transport. The capability to cross the BBB has an impact on the overall distribution systemically, as well as the possible central effects. It might also be possible that benzoic acid analogs (DCF5, DCF6, and DCF8) contain their central as well as peripheral pharmacological effects, and those with a slightly lower BBB value (DCF4 and DCF1) have a more balanced distribution. Toxicity-related measures (HERGI, AMEST, NC, BD, and AOT) provide insight into the safety and tolerability of the drugs. The lack of cardiac arrhythmia was proven by the high safety margins (0.881–0.993) in all the analogs of the HERG inhibition, which is an indicator of the possible cardiotoxicity by potassium ion channel blockage. Among the Ames test probabilities (0.518–0.913), it was discovered that most of the substances are not mutagenic, suggesting that they are genetically safe. All analogs had low carcinogenicity possibilities, with sufficient non-carcinogenic (NC) possibilities (0.481–0.807).

All of the analogs showed promising results in terms of biodegradability (BD), with values ranging from 0.964 to 1.000. This suggests they are well metabolized in the body and are unlikely to persist in the environment. Biodegradability, a crucial predictor for sustainable pharmacology, is the ability of such compounds to biodegrade, and thus, they are probably less likely to accumulate in tissues or ecosystems. The value of acute oral toxicity (AOT) of 0.507 to 0.760 reveals mild to moderate toxicity. Compared with the parent drug DCF (0.760), DCF analogs DCF4 (0.528), DCF5 (0.609), and DCF6 (0.540) exhibited lower AOT values, indicating improved oral safety and tolerability.

3.9. PASS prediction and drug likeness

The biological importances of DCF and its structurally modified derivatives are evaluated probabilistically by the prediction of activity spectra for substances (PASS) findings. The values of Pa (probability "to be active") and Pi (probability "to be inactive") reflect the chance that a chemical exhibits a given pharmacological or toxicological action.[47,48] Pa > 0.5 generally indicates a rather high likelihood of experimentally detecting the anticipated actions.[49] DCF showed strong antipyretic (0.827), anti-inflammatory (0.791), and analgesic (0.501) effects among its pharmacological endpoints (Table 2). These reflect the well-documented therapeutic profile of DCF as a powerful NSAID in clinical trials. Although there were some variations, the majority of derivatives maintained these fundamental activities. DCF3 has the strongest anti-inflammatory potential (0.757) and the highest antipyretic activity (0.868), suggesting that its structural modification may enhance NSAID-like biological actions. The anti-inflammatory effects of DCF1, DCF2, and DCF7 were moderate to high (Pa: 0.665–0.739), indicating that changes at specific functional groups maintained the inhibitory action of COX. At the same time, alterations impacting ligand–protein interactions are likely responsible for the decrease in antipyretic activity, as indicated by the decrease in antipyretic predictions for DCF4, DCF5, and DCF6 (Pa: 0.344–0.387). PASS also predicted a few toxicology endpoints, which are important for the assessment of the drug safety profile. Pa-values of DCF were extremely high for GH (0.966), HT (0.841), UC (0.876), NT (0.650), and HP (0.886). The generation of reactive metabolites, impaired prostaglandin biosynthesis, and inactivation of COX-2 have all been described as DCF-related toxicological threats. The probability of ulceration as well as hepatotoxicity is higher for DCF2, DCF4, and DCF6, with values ranging from (Pa = 0.626 to 0.861) and (Pa = 0.347 to 0.773), implying that these changes may reduce its major dose-limiting side effects.

However, DCF6 and DCF7 exhibited a modest decrease in hepatotoxicity and ulcerogenic activity, indicating that specific structural changes may ameliorate toxicity to some extent. Toxicological outcomes, including gastrointestinal hemorrhage (0.669) and ulceration (0.412), were substantially less likely in DCF8, where multiple actions were not anticipated. It appears that the toxicity profile could be less hazardous; however, there are several structural novelty predictions that were not considered in the PASS preparation.

Drug-likeness is an important indicator for evaluating the pharmaceutical candidacy of DCF and its analogues.[47,50,51] Oral bioavailability, solubility, and permeability of the compounds are evaluated by several properties, such as Lipinski, Ghose,

Table 2 Prediction of biological activities of DCF using PASS[a]

Name	AP	AI	OI	AG	GH	AA	AS	HT	UC	NT	HP
DCF	0.827	0.791	0.636	0.559	0.966	0.526	0.501	0.841	0.876	0.650	0.886
DCF1	0.607	0.716	0.344	0.196	0.916	0.457	0.338	0.722	0.715	0.319	0.740
DCF2	0.796	0.739	0.338	0.249	0.883	0.406	0.358	0.773	0.861	0.613	0.799
DCF3	0.868	0.757	0.354	0.394	0.947	0.522	0.483	0.752	0.932	0.613	0.855
DCF4	0.387	0.589	0.257	0.278	0.834	0.612	0.222	0.347	0.779	0.295	0.506
DCF5	0.387	0.589	0.257	0.278	0.834	0.612	0.222	0.347	0.779	—	0.506
DCF6	0.344	0.665	0.296	0.178	0.748	0.243	0.293	0.485	0.626	0.383	0.661
DCF7	0.485	0.677	0.304	0.392	0.846	0.296	0.279	0.717	0.505	0.596	0.845
DCF8	—	0.779	—	0.257	0.669	—	0.568	0.281	0.412	0.394	0.281

[a] AP = antipyretic, AI = anti-inflammatory, OI = omptin inhibitor, AG = anesthetic general, GH = gastrointestinal hemorrhage, AA = antiarthritic, AS = analgesic, HT = hepatotoxic, UC = ulceration, NT = nephrotoxic, HP = hepatitis.

Veber, Egan, and Muegge rules.[52–54] The bio-availability score (BAS), number of hydrogen bond donors (NHD), and the number of hydrogen bond acceptors (NHA) are also used to assess the overall drug-likeness. With respect to DCF, as shown in Y (yes) for each of the Lipinski, Ghose, Veber, Egan, and Muegge rules, a BAS value equal to 0.85 is also reported, indicating CDF has good oral bioavailability (Table S8). NHD and NHA are 2, which fall within an optimal region, indicating DCF has a reasonable combined lipophilic/hydrophilic profile for oral drug absorption. In the analogues, DCF1 and DCF2 have drug-likeness similar to DCF, having no number of rule violations according to Lipinski and Ghose indicating that these obeyed prime rules for the drug-like properties for oral bioavailability. However, DCF1 and DCF2 have slightly decreased BAS (0.55) and more HB donors (3), which could cause their higher hydrophilic nature and potentially lower cell permeability than those of DCF. In contrast, DCF3, DCF4, DCF5, and DCF6 break certain rules, especially the Veber, Ghose, and Egan ruling. The infringements are expressed in the BAS values 0.55–0.56, thereby suggesting that these derivatives may have lower bioavailability. Moreover, for some of these analogs, the hydrogen donor number rises to 3–4, which can lead to a change in membrane permeation and ability to cross the lipid bilayer. There may be a correlation between BAS in DCF5 and its low permeability and poor oral bioavailability because of the high number of H-bond donors (1). Apart from that, DCF7 is part of a different dataset class with a BAS of 0.55, which goes against Lipinski and Egan's guidelines. This suggests that DCF7 might have low solubility and permeability, even while it retains an acceptable amount of hydrogen bond acceptors (1).

Radar images comparing DCF and its variations based on their similarity in chemical and physical features are shown in Fig. S7. These characteristics are summarized as follows in six important ways: lipophilicity, flexibility, size, polarity, insaturation, and insolubility. The similarities and differences between these substances, in terms of molecular structure and medicinal efficacy, are shown by the radar plot. The DCF profile is well-balanced, and the parameters, particularly LIPO and polarity, undergo small adjustments. Its ability to enter cells and interact with their targets may be a result of these characteristics. The similarity in their profiles suggests that DCF1 and DCF2 likely have similar molecular actions that are not heavily dependent on their stiffness or hydrophobicity. Differentiating DCF1 and DCF2 is as simple as looking at the polarity-dependent peak locations and the lengths of the various phase areas. There is more FLEX in DCF3 and less LIPO in DCF4, compared to DCF. Their solubility and ability to cross cell membranes are both impacted by this, which could make absorption more of a challenge. Being smaller and having a much lower LIPO makes DCF5 more hydrophilic. The drug's distribution and absorption may be affected, making it more difficult to receive when given orally. Without DCF, none of them had a higher LIPO. They may disintegrate differently depending on this property, which in turn affects their ability to penetrate tissues and interact with biological membranes.

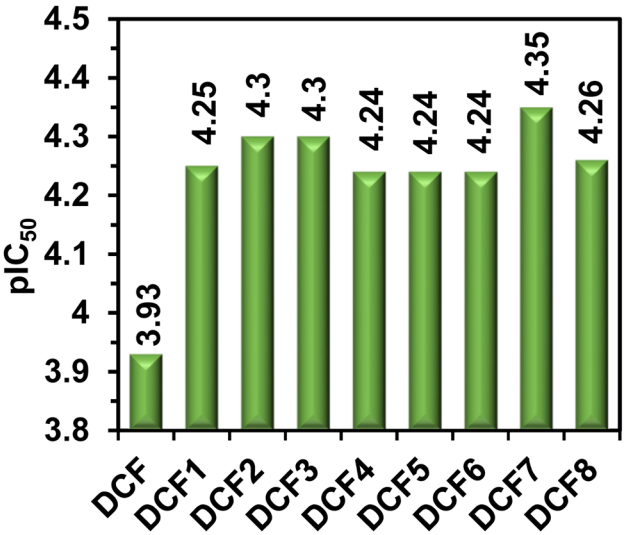

Fig. 9 pIC_{50} studies of DCF and its derivatives.

3.10. pIC_{50} studies

For the pIC_{50} studies, QSAR methods are used to estimate key properties for the biological and pharmacological activity of new compounds.[55,56] These procedures rely upon multivariate quantitative mathematical approaches, where a complex relationship is established between independent molecular descriptors and pIC_{50} values (as the dependent variable that stands for compound biological potency). The independent descriptors include Chiv5, bcutm1, MRVSA9, MRVSA6, PEOEVSA5, GATSv4, J and Diametert.[57] These descriptors are derived from the physicochemical and morphological characteristics of the compound (molecular size, shape, and electronic distribution), which have been shown to play a critical role in a compound's biological effectiveness.

pIC_{50} values of DCF and its derivatives are presented in Fig. 9 and Table S9, with the pIC_{50} value of DCF (3.93) much lower than that of its derivatives. The typical range for pIC_{50} values of drugs is from 4.0 to 10.0.[58] The derivatives DCF1–DCF8 show pIC_{50} from 4.24 to 4.35. This suggests that these derivatives have a stronger binding affinity or activity than DCF.

In conclusion, DCF7 (pIC_{50} = 4.35) has the highest pIC_{50} value for all its analogs, and the lowest ones are shown for DCF4, DCF5, and DCF6 with values of 4.24, respectively. Hence, DCF is the only derivative for which pIC_{50} values do not cover all of the standard range. This suggests that the structural changes of DCF derivatives are ascribed to enhanced biological activity, which may contribute to the potency of this compound.

4. Conclusion

An in-depth *in silico* analysis of DCF and eight new designed derivatives, as well as their electronic properties, thermodynamic stability, binding characteristics, and pharmacokinetic suitability, is analyzed. The thermodynamic profiles of the derivatives indicated that most metabolites have total electronic energies lower than those found for the parent drug (DCF), thus

indicating improved stability. Derivatives DCF2, DCF3, and DCF8 showed observing stabilization of atomic charge, while modest changes in the dipole moments for some analogs suggest an increased polarity and stronger interactions with other biological targets. The FMO analysis demonstrated that both DCF3 and DCF6 possess lower HOMO–LUMO energy gaps, chemical softness, and sensitivity than the other analogues, which suggests the former's higher reactivity and polarizability. These results were further supported by UV-visible absorption spectral red shifts and DOS analyses, suggesting increased conjugation length and better ability of charge transfer. All analogues still had their main groups intact, as verified by FT-IR analyses. The molecular docking studies with COX-2 demonstrated that all the analogs compared to DCF showed relatively good affinity. The binding profile of DCF6 indeed appeared most favorable, and subsequent 100 ns MD simulations confirmed stable protein–ligand complexes. ADMET analysis also exhibited high intestinal absorption, efficient renal elimination, and promising BBB permeability, together with low acute oral toxicity by DCF4, DCF5, and to a lesser extent by DCF6. PASS prediction supported retaining core NSAID properties and minimizing hepatotoxicity and ulcerogenic risk profile for specific derivatives. The findings indicate that the selective structural modification of DCF may enhance stability, COX-2 affinity, and anticipated safety. Though DCF3 demonstrates superior intrinsic electronic stability and reactivity, its alternate binding mode likely prevents it from functioning as a classical COX-2 inhibitor. Consequently, DCF2, DCF4, and DCF6 are the most promising analogues requiring further experimental validation through *in vitro*, *in vivo*, and pharmacological studies.

Author contributions

Ibrahim Khalil, Sadia Zaman: writing – original draft, visualization, methodology, investigation, formal analysis. Ishrat Jahan Aliza, Marjia Rahman Tanny, Tasnim Hasan: writing – original draft, methodology, investigation. Monir Uzzaman: conceptualization, supervision, project administration, investigation, writing – review & editing, methodology, validation, data curation.

Conflicts of interest

The authors declare that neither their personal ties nor any known financial conflicts influenced this publication.

Data availability

All data generated or analyzed during this study are included in this published article [and its supplementary information (SI) files]. Supplementary information is available. See DOI: https://doi.org/10.1039/d6ra01053a.

Acknowledgements

We are extremely grateful to the 'Computer in Chemistry and Medicine Laboratory' in Dhaka, Bangladesh, for their invaluable advice and expertise, which significantly enhanced the outcome and direction of our study.

References

1 S. Bindu, S. Mazumder and U. Bandyopadhyay, *Biochem. Pharmacol.*, 2020, **180**, 114147, DOI: 10.1016/j.bcp.2020.114147.
2 M. Dronik and M. Stasevych, *Sci. Pharm.*, 2025, **93**, 31, DOI: 10.3390/scipharm93030031.
3 F. Bariguian, R. Marina and F. M. Hagen, *Rheumatol. Ther.*, 2020, **7**, 217–236, DOI: 10.6084/m9.figshare.11791470.
4 R. Altman, B. Bosch, K. Brune, P. Patrignani and C. Young, *Drugs*, 2015, **75**, 859–877, DOI: 10.1007/s40265-015-0392-z.
5 T. J. Gan, *Curr. Med. Res. Opin.*, 2010, **26**, 1715–1731, DOI: 10.1185/03007995.2010.486301.
6 A. R. Sallmann, *Am. J. Med.*, 1986, **80**, 29–33, DOI: 10.1016/0002-9343(86)90076-8.
7 M. Hofer, Z. Hoferová and M. Falk, *Molecules*, 2019, **24**, 4019, DOI: 10.3390/molecules24224019.
8 G. M. Pacifici, *Biomed. J. Sci. Tech. Res.*, 2024, **56**, 48609–48621, DOI: 10.26717/bjstr.2024.56.008918.
9 P. R. Hatwar, R. L. Bakal, A. N. Motwani, R. L. Bakal, D. A. Deulkar and A. A. Gupta, *World J. Pharm. Pharmaceut. Sci.*, 2024, **29**, 341–355, DOI: 10.20959/wjpps20242-26532.
10 Z. R. Chen, B. K. Chen, P. Li and K. Feng, *BMC Musculoskeletal Disord.*, 2025, **26**, 230, DOI: 10.1186/s12891-025-08465-7.
11 J. D. Smith, S. F. Naoom, L. Saldana, *et al.*, *Prev. Sci.*, 2024, **25**, 1–9, DOI: 10.1007/s11121-023-01617-y.
12 C. Nelson, *Ther. Clin. Risk Manage.*, 2011, **7**, 207–211, DOI: 10.2147/tcrm.s12498.
13 A. N. Zaid, A. M. Fadda, S. Nator and A. Qaddumi, *J. Pharm. Investig.*, 2011, **41**, 211–215, DOI: 10.4333/KPS.2011.41.4.211.
14 F. W. D. Tai and M. E. McAlindon, *Clin. Med.*, 2021, **21**, 131–134, DOI: 10.7861/CLINMED.2021-0039.
15 L. D. Bash, K. White, M. D. Patel, *et al.*, *Cardiol. Ther.*, 2019, **8**, 329–343, DOI: 10.1007/s40119-019-00147-5.
16 M. Schmidt, H. T. Sørensen and L. Pedersen, *BMJ*, 2018, **362**, k3426, DOI: 10.1136/bmj.k3426.
17 S. a. d. M. Khatlan, R. H. Hamad, O. M. Mohammed and A. Y. Khudhair, *South Asia Res. J. Biol. Appl. Biosci.*, 2024, **6**, 228–234, DOI: 10.36346/sarjbab.2024.v06i06.004.
18 E. Khalil, N. Fahmy EL-baroudy, L. Mahgoub and M. Nageeb, *Zagazig Univ. Med. J.*, 2025, **31**, 56–61, DOI: 10.21608/zumj.2024.277963.3265.
19 L. Lonappan, S. K. Brar, R. K. Das, M. Verma and R. Y. Surampalli, *Environ. Int.*, 2016, **96**, 127–138, DOI: 10.1016/j.envint.2016.09.014.
20 R. E. Green, M. A. Taggart, D. Das, D. J. Pain, C. Sashi Kumar, A. A. Cunningham and R. Cuthbert, *J. Appl. Ecol.*, 2006, **43**, 949–956, DOI: 10.1111/j.1365-2664.2006.01225.x.

21 J. W. Mallord, S. Ranade, K. P. Bhusal, A. B. M. S. Alam, M. J. I. Chaudhry, S. S. Chakraborty, B. Subbaiah, D. L. Bohra, A. Dube, R. Shringarpure, I. P. Chaudhary, A. B. Joshi, D. B. Rana, D. C. Thakuri, H. L. Dangaura, K. Z. Azmiri, S. Ahmed, T. Zakir, S. Ahmed, H. Fatima, M. C. RahimA, C. G. R. Bowden and R. E. Green, *Bird. Conserv. Int.*, 2025, **35**, e38, DOI: 10.1017/S0959270925100270.
22 M. Joshi, I. Pathan, A. Sahu, A. Raza, Y. Sahu and N. Khatoon, *J. Pharm. Sci. Comput. Chem.*, 2025, **1**, 246–266, DOI: 10.48309/jpscc.2025.535670.1020.
23 L. E. Clegg and F. Mac Gabhann, *Pharmacol. Res.*, 2015, **99**, 149–154, DOI: 10.1016/j.phrs.2015.06.002.
24 M. Uzzaman and M. N. Uddin, *Daru J. Pharm. Sci.*, 2019, **27**, 71–82, DOI: 10.1007/s40199-019-00243.
25 M. K. Hasan, S. Akhter, K. Fatema, M. R. Hossain, T. Sultana and M. Uzzaman, *Inform. Med. Unlocked*, 2023, **36**, 1–11, DOI: 10.1016/j.imu.2023.101159.
26 M. Omor Farque, R. M. Islam, M. F. R. Joni, M. Akter, S. Akter, M. D. Islam, M. D. J. B. Salim, A. Abdul Aziz, E. Kabir and M. Uzzaman, *Inform. Med. Unlocked*, 2025, **53**, 1–12, DOI: 10.1016/j.imu.2025.101617.
27 M. Uzzaman, M. K. Hasan, S. Mahmud, K. Fatema and M. M. Matin, *Inform. Med. Unlocked*, 2021, **25**, 1–11, DOI: 10.1016/j.imu.2021.100677.
28 E. N. Feinberg, E. Joshi, V. S. Pande and A. C. Cheng, *J. Med. Chem.*, 2020, **63**, 8835–8848, DOI: 10.1021/acs.jmedchem.9b02187.
29 D. S. Druzhilovskiy, A. V. Rudik, D. A. Filimonov, T. A. Gloriozova, A. A. Lagunin, A. V. Dmitriev, P. V. Pogodin, V. I. Dubovskaya, S. M. Ivanov, O. A. Tarasova, V. M. Bezhentsev, K. A. Murtazalieva, M. I. Semin, I. S. Maiorov, A. S. Gaur, G. N. Sastry and V. V. Poroikov, *Russ. Chem. Bull.*, 2017, **66**, 1832–1841, DOI: 10.1007/S11172-017-1954-X.
30 M. Uzzaman, M. K. Hasan, S. Mahmud, A. Yousuf, S. Islam, M. N. Uddin and A. Barua, *Inform. Med. Unlocked*, 2021, **25**, 1–10, DOI: 10.1016/j.imu.2021.100706.
31 A. U. Jan, K. Khan, T. Shah, N. Ahmad and H. Ur Rashid, *Orbital*, 2025, **17**, 7–19, DOI: 10.17807/orbital.v17i1.21586.
32 A. Jinich, D. Rappoport, I. Dunn, *et al.*, *Sci. Rep.*, 2014, **4**, 7022, DOI: 10.1038/srep07022.
33 T. M. Laue, S. J. Shire, T. M. Laue and S. J. Shire, *J. Pharm. Sci.*, 2020, **109**, 154–160, DOI: 10.1016/j.xphs.2019.10.045.
34 T. H. Ho, H. D. Tong and T. T. Trinh, *Sci. Rep.*, 2024, **14**, 1, DOI: 10.1038/s41598-024-67720-4.
35 N. C. Garbett and J. B. Chaires, *Expert Opin. Drug Discovery*, 2012, **7**, 299–314, DOI: 10.1517/17460441.2012.666235.
36 M. N. Uddin, *et al.*, *J. Mol. Struct.*, 2020, 1206, DOI: 10.1016/j.molstruc.2020.127678.
37 A. A. Benjamine, B. A. Lucie, Y. K. Denis and B. E. H. Sawaliho, *Comput. Chem.*, 2019, **07**, 95–105, DOI: 10.4236/cc.2019.74007.
38 C. Ravikumar, I. H. Joe and V. S. Jayakumar, *Chem. Phys. Lett.*, 2008, **460**, 552–558, DOI: 10.1016/j.cplett.2008.06.047.
39 R. N. Devi, A. D. Stephen, P. Justin, K. Saravanan, P. Macchi and C. Jelsch, *J. Mol. Struct.*, 2019, **1196**, 42–53, DOI: 10.1016/j.molstruc.2019.06.027.
40 Y. G. Sıdır and İ. Sıdır, *J. Fluoresc.*, 2025, **35**, 8269–8287, DOI: 10.1007/s10895-025-04154-9.
41 M. Shah, M. Patel, M. Shah, M. Patel and M. Prajapati, *Intell. Pharm.*, 2024, **2**, 589–595, DOI: 10.1016/j.ipha.2024.03.001.
42 B. Anusha and G. Rao Kamala, *J. Pharma Insight Res.*, 2025, **3**, 140–151, DOI: 10.69613/29zcv966.
43 A. Tiwari and S. Singh, Computational approaches in drug designing, in *Bioinformatics: Methods and Applications*, Elsevier BV, 2022, pp. 207–217, DOI: 10.1016/B978-0-323-89775-4.00010-9.
44 G. N. Pairas and P. G. Tsoungas, *ChemistrySelect*, 2016, **1**, 4520–4532, DOI: 10.1002/slct.201600770.
45 D. E. Arthur and A. Uzairu, *J. King Saud Univ., Sci.*, 2019, **31**, 1151–1166, DOI: 10.1016/j.jksus.2019.01.011.
46 R. B. O. Ouma, S. M. Ngari and J. K. Kibet, *Discover Public Health*, 2024, **21**, 1–31, DOI: 10.1186/s12982-024-00229-3.
47 M. Khaiitova, *J. Clin. Med. Kaz.*, 2023, **20**, 60–67, DOI: 10.23950/jcmk/13541.
48 A. A. Oliveira Filho, H. M. B. Fernandes, T. J. C. F. Assis, D. R. P. Meireles, O. Edeltrudes, E. O. Lima and H. L. F. Pêssoa, *Int. J. Pharmacogn. Phytochem. Res.*, 2015, **7**, 431–434.
49 A. Lagunin, A. Stepanchikova, D. Filimonov and V. Poroikov, *Bioinformatics*, 2000, **16**, 747–748, DOI: 10.1093/bioinformatics/16.8.747.
50 W. Zhu, Y. Wang, Y. Niu, L. Zhang and Z. Liu, *Health Data Sci.*, 2023, **3**, 0098, DOI: 10.34133/hds.0098.
51 G. Sampat, S. S. Suryawanshi, M. S. Palled, A. S. Patil, P. Khanal and A. S. Salokhe, *Adv. Pharmacol. Pharm.*, 2022, **10**, 234–246, DOI: 10.13189/app.2022.100402.
52 L. El Mchichi, A. El Aissouq, T. Lakhlifi and M. Bouachrine, *Chem. Rev. Lett.*, 2021, **4**, 145–152, DOI: 10.22034/crl.2021.262806.1098.
53 S. Pathania and P. K. Singh, *Expert Opin. Drug Metab. Toxicol.*, 2021, **17**, 351–354, DOI: 10.1080/17425255.2021.1865309.
54 O. Ursu, A. Rayan, A. Goldblum and T. I. Oprea, *WIREs Comput. Mol. Sci.*, 2011, **1**, 760–781, DOI: 10.1002/wcms.52.
55 B. A. Umar, A. Uzairu, G. A. Shallangwa, and U. Sani, *Network Modeling Analysis in Health Informatics and Bioinformatics*, 2019, vol. 8, p. 22, DOI: 10.1007/s13721-019-0202-8.
56 S. Kralj, M. Jukič and U. Bren, *Encyclopedia*, 2023, **3**, 501–511, DOI: 10.3390/encyclopedia3020035.
57 E. Kabir, M. R. O. K. Noyon and M. Uzzaman, *Pharmacogn. J.*, 2023, **15**, 194–207, DOI: 10.5530/pj.2023.15.29.
58 S. Tukur, G. A. Shallangwa and A. Ibrahim, *Heliyon*, 2019, **5**, 11, DOI: 10.1016/j.heliyon.2019.e02859.